Size Effect on Shear Fracture and Fragmentation of a Fe$_{57.6}$Co$_{14.4}$B$_{19.2}$Si$_{4.8}$Nb$_4$ Bulk Metallic Glass**

By *Fu-Fa. Wu, Zhe-Feng Zhang,* Bao-Long Shen, Scott Xing-Yuan Mao* and *Jürgen Eckert*

Since the discovery of the first bulk metallic glass (BMG), numerous alloy systems with excellent glass-forming ability have been developed to date.[1–4] According to their deformation and fracture modes at room temperature, they are generally divided into two classes: ductile BMGs and brittle BMGs.[4–7] The typical deformation and fracture features of ductile BMGs are the formation of shear bands and shear fracture with a well developed vein pattern on the fracture surface.[8,9] However, brittle BMGs always fail in split and fragmentation modes, exhibiting mirror and hackle regions on the fracture surface.[6,10–13] Recently, nano-scale features were observed in the mirror region on the fracture surface of brittle BMGs.[10,12,14–20] It was argued that these features correspond to nano-scale plasticity, and the fracture toughness was calculated according to these nano-scale feature.[12,20] Moreover, it was proposed that the fracture in brittle BMGs might also proceed through a local softening mechanism like in ductile BMGs but at smaller length scale.[10,12] However, other researchers regarded these nano-scale features as a fingerprint of wavy cleavage fracture caused by a dynamic instability.[14,15] However, it is still unknown what intrinsically controls this brittle fracture behavior.

In this work, the deformation and fracture behavior of a brittle Fe$_{57.6}$Co$_{14.4}$B$_{19.2}$Si$_{4.8}$Nb$_4$ BMG was investigated to reveal the fundamental nature of the fracture for those brittle BMGs. It is found that shear banding is a general deformation feature for all BMGs, including the brittle BMGs, and the shear deformation becomes more pronounced for samples with smaller size. Fragmentation conceals the shear deformation in case of large size samples, but becomes less pronounced for a small sample size.

Figure 1 shows the stress-strain curves of Samples S1 and S2 with different dimensions. For the Sample S1 with a dimension of φ 2.0 mm × 4 mm, the fracture strength is about 4274 MPa, and the plasticity is about 0.4 %. For the Sample S2 with a nominal dimension of 1.0 × 1.0 × 2.0 mm^3, the fracture strength is 4072 MPa, which is ~ 200 MPa lower than that of the Sample S1, and the plasticity is around 0.8 %, i.e. about twice that of Sample S1. These results agree well with previous findings.[21,22] In addition, pronounced serrated flow is visible for the stress-strain curves of Sample S2, with a serrated flow stress amplitude of about 128 MPa. However, for the Sample S1, there is no obvious serrated flow.

It was found that the Sample S1 failed by a fragmentation mode with a bombing sound, producing a lot of fine fragments,[6,11] as shown in Figure 2(a). Mirror and hackle regions were formed on the fracture surface (see Fig. 2(b)), which is

[*] Prof. Z. F. Zhang, Dr. F. F. Wu
Shenyang National Laboratory for Materials Science
Institute of Metal Research
Chinese Academy of Sciences
72 Wenhua Road, Shenyang 110016, China
E-mail: zhfzhang@imr.ac.cn

Prof. B. L. Shen
Ningbo Institute of Material Technology and Engineering
Chinese Academy of Sciences
Ningbo 315040, China

Prof. S. X. Mao
Department of Mechanical Engineering and Materials Science
University of Pittsburgh
648 Benedum Hall, Pittsburgh, PA 15261, USA

Prof. J. Eckert
IFW Dresden, Institute for Complex Materials
P.O. Box 27 01 16, D-01171 Dresden, Germany
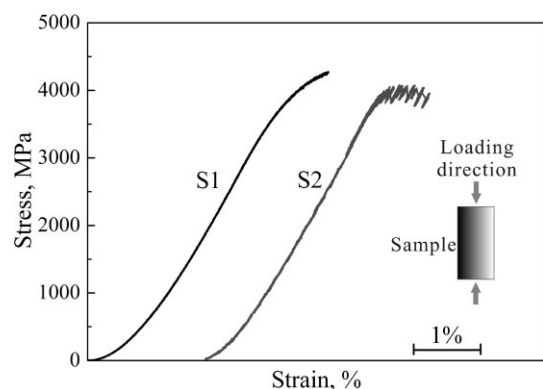and TU Dresden, Institute of Materials Science
D-01062 Dresden, Germany.

Fig. 1. Stress-strain curves of the Samples S1 and S2. The sample size is 2.0 mm in diameter and 4.0 mm in height for the Sample S1, and 1.0 × 1.0 × 2.0 mm^3 for the Sample S2.
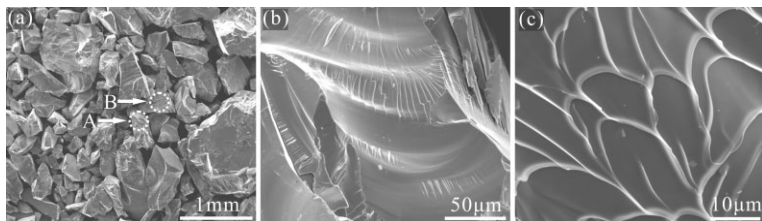
Fig. 2. Fracture features observed for the Sample S1 after failure. (a) Numerous fragments formed during the fracture; (b) the predominant brittle fracture feature in the fragment marked with A in (a); (c) vein pattern showing some ductile fracture features in few fragments marked with B in (a).

the typical fracture feature of brittle metallic glasses.[12,14,23] By carefully observing fragment by fragment, it was found that some vein patterns were also formed on the fracture surfaces in a few fragments (see Fig. 2(c)), which is the typical shear deformation and fracture feature of ductile metallic glasses, such as most Zr-, Cu-, and Pd-based metallic glasses.[9,24,25] In contrast to the predominantly brittle fracture by fragmentation, the ductile fracture surface features with vein pattern are very limited. The vein pattern is 10–20 μm in length, which is about half of the size found for Zr-, Cu-, or Ti-based metallic glasses.[9,26,27] This to some extent implies that the viscosity in the shear bands of the present Fe-based metallic glass is larger than that of Zr-, Cu-, or Ti-base metallic glasses.

In contrast to the fragmentation failure mode in the Sample S1, the Sample S2 shows a typical shear deformation (a major shear band can be seen in Fig. 3(a)). The shear angle is around 41.5°, similar to that of other ductile metallic glasses.[9] Higher resolution SEM images of the selected Region A (marked in Fig. 3(a)) shows that a shear offset of 13.4 μm formed in the deformed Sample S2, as displayed in Figure 3(b). In addition to the shear bands, it is interesting to find that some cracks were formed along the loading direction on the surface of the Sample S2, as indicated in Figure 3(c) and 3(d). The tips between the cracks and the shear bands are severely bend, and forced to penetrate into the cracks (see Fig. 3(c)). The cracks even cross the shear bands with no deflection in their propagation direction (see Fig. 3(d)).

According to these findings, it is clear that the Sample S1 with larger size displays predominant fragmentation failure with only some weak shear failure features, as shown in Figure 2. However, in sharp contrast to Sample S1, Sample S2 with small size exhibits a predominant shear failure with an only weak tendency for fragmentation failure, as shown in Figure 3. Apparently, there is a strong size effect affecting the deformation and fracture processes for an identical Fe-based metallic glass even when the sample dimensions are in the millimeter range. Careful consideration of the results in Figure 2 and Figure 3 suggests that the Sample S1 with larger size still deforms by shear, but the shear deformation is completely concealed by the numer-

ous fragments (see Fig. 2(a)). In order to clarify if shear deformation in fact occurred in the Sample S1, a steel tube was used to prevent fragmentation and to retain the whole fracture feature at the instant of failure, as illustrated in Figure 4(a). The steel tube had an inner diameter slightly larger than the diameter of the Sample S1 so that the elastic and plastic deformation of the sample was not affected. This assembly is completely different from a similar previous test set-up that produced a strong constraint to the sample during the deformation.[28,29] After failure, the Sample S1 was taken out from the steel tube. Figures 4(b), 4(c) and 4(d) show the deformation and failure features of the Sample S1 encapsulated by the protecting of the steel tube. A major shear band was formed, which penetrates through the whole sample, as shown in Figures 4(b) and 4(c). In addition, the whole sample is covered by plenty of fragments, which implies that fragmentation is still the predominant failure mode, as shown in Figure 4(d).

Further investigation indicates that the deformation and fracture phenomena described above also occurs in brittle Co- and Mg-based BMGs.[30] Therefore, the mixture of shear fracture and fragmentation fracture seems to be a general fracture phenomenon in brittle BMGs. As is well known, the elastic deformation behavior can influence the subsequent plastic deformation and fracture, and Poisson's ratio (v), which has been considered to be related to intrinsic brittleness and ductility of bulk metallic glasses.[31,32] Small v means that the atoms can hardly rearrange themselves to accommodate the shear strain without a drastic disturbance in bonding configurations, and a large v indicates easy atomic rearrangements.[32] Therefore, a small v prevents the tip of a shear band
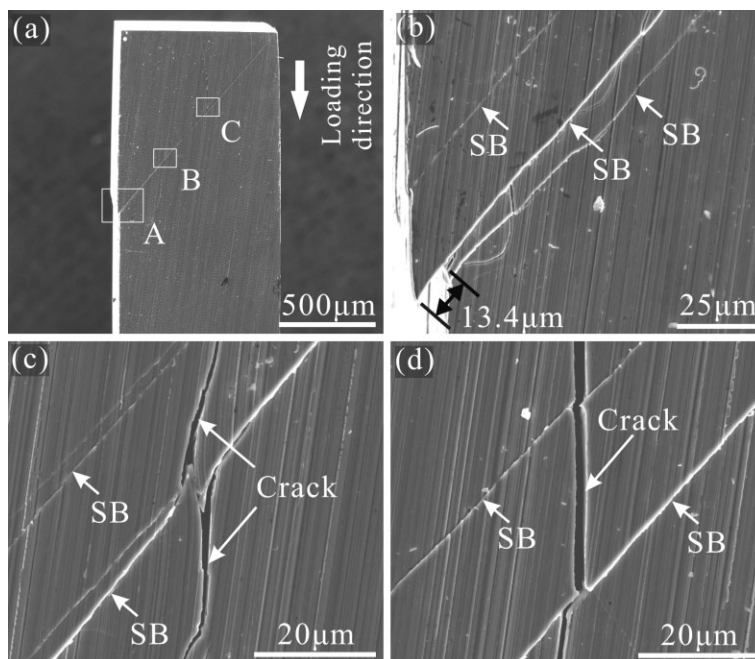

Fig. 3. Fracture features in the Sample S2 after failure. (a) and (b) Shear bands and an obvious shear offset formed in the Sample S2; (c) and (d) cracks formed along the loading direction.
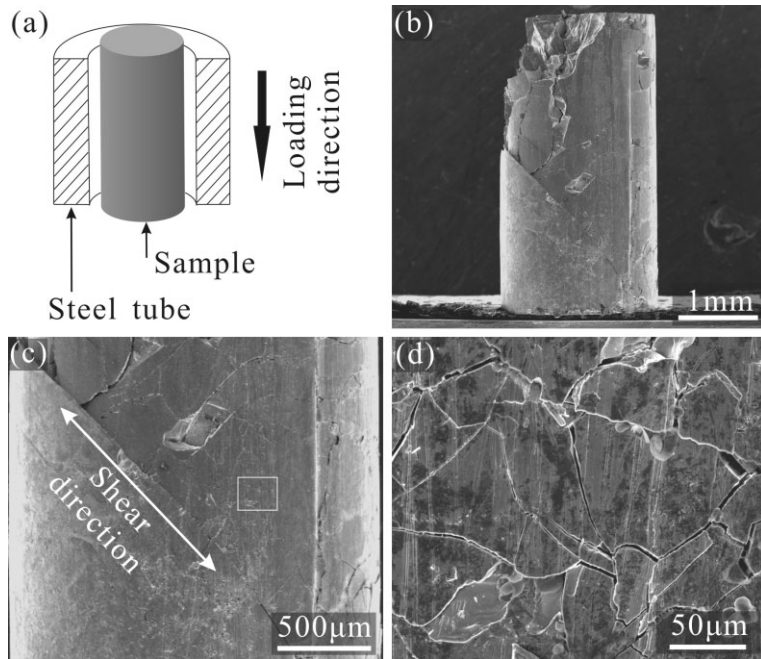
Fig. 4. (a) Schematic illustration of the protected compression test. (b) and (c) Shear band and fragmentation formed in the whole Sample S1; (d) high-resolution SEM image showing the fragmentation in the frame marked in (c).

from extending, resulting in initiation of a crack. When v decreases below a critical value of 0.31-0.32, BMGs will exhibit ductile fracture features.[31] For most Fe-based BMGs,[31,32] v is significantly smaller than the critical value of 0.31–0.32. Thus, the present Fe-based BMG tends to form cracks rather than shear bands during the deformation even in the elastic regime. When the cracks completely propagate through the sample, a crack network forms and the sample disintegrates into numerous fragments, leading to the occurrence of the so-called fragmentation fracture.

The present results also suggest that there exists an obvious size effect on the deformation and fracture mode of the Fe-based BMG, as shown in Figure 1, Figure 2, and Figure 3. To understand this issue, the shear deformation behavior of metallic glass needs to further consider here. Generally speaking, the room-temperature plastic strain of metallic glass is produced by the shear offset of two undeveloped parts separated by the localized shear band.[24] With the shear band propagating, the shear offset increases, so does the plastic strain. When a shear band propagates to a critical length, it develops maturely with a low bonding strength,[33] leading to the final catastrophic fracture along shear band. Thus, there should be a "critical shear offset (λ_c)", above which the shear band starts to be unstable, leading to the final shear fracture.[34] The critical shear offset is a direct parameter phenomenally reflecting the stable shear capability. The length of critical shear offset is equal to that of the smooth region at the initial fracture surface of metallic glass sample after fracture.[34–36] Therefore, it is suggested that the shear deformation capability of metallic glass is related to the critical shear offset: the plastic strain of metallic glass at fracture increases

linearly with increasing critical shear offset. Furthermore, based on the concept of critical shear offset, the overall deformation behavior of metallic glass can be categorized into two regimes with regard to the sample size. At first, if the sample size w is significantly larger than the critical shear offset (λ_c), the shear offset produced by propagation of shear band will reach the critical one (λ_c), and catastrophic failure will occur. Therefore the plastic strain at failure (ε_p) can be calculated by the sample size w (the aspect ratio is 2) and the critical shear offset λ_c, which is expressed as

$$\varepsilon_p = \lambda_c \cos\theta/2w, \tag{1}$$

where θ is the shear angle between the shear plane and the loading direction, and w is the sample size (diameter or width of the sample). For a given metallic glass, the critical shear offset λ_c is constant. Therefore, according to Equation 1, a decreasing sample size w will obviously increase the plasticity of the metallic glass, as shown in Figure 1 and Figure 3. Substituting $\lambda_c \approx 15$ μm, θ=41.5°, and w=1000 μm (1.0 mm) into Eq. (1), one can calculate a plastic strain of ε_p=0.6 % for the Fe-based BMG Sample S2, which is very close to the measured value of 0.8 %. The difference between the calculated and the measured plasticity is reasonable when taking secondary shear bands and the pseudo-plasticity caused by the fragmentation into account.[4]

On the other hand, due to the highly localized shear deformation in metallic glass, the elastic energy stored before fracture is mostly dissipated on the fracture surface as heat.[37] Some results showed that heat plays an important role in the softening of a shear band and the catastrophic fracture of metallic glass.[38] If the aspect ratio of sample is 2, the energy density of the shear fracture surface caused by the elastic energy release during the fracture process can be approximately expressed as

$$\delta = \frac{1}{2}\sigma_e\varepsilon_e V/A = w\sigma_e\varepsilon_e \sin\theta \tag{2}$$

Where σ_e is the maximum elastic stress (elastic limit), ε_e is the maximum elastic strain, V is the volume of the sample, a is the area of the shear plane, w is the sample size (diameter or width), and θ is the shear angle between the shear plane and the loading direction. According to Equation 2, it is clear that the energy density dissipated on the shear fracture surface decreases linearly with decreasing sample size (w). Thus, a decreasing sample size will enhance the stability of the shear band, i.e. it becomes difficult to render the shear band to propagate maturely to form a crack. Therefore, with decreasing sample size, shear deformation becomes more likely.

In summary, both shear fracture and fragmentation can occur in a brittle $Fe_{57.6}Co_{14.4}B_{19.2}Si_{4.8}Nb_4$ BMG. For samples with larger size, the shear deformation features are concealed

by the predominant fragmentation fracture. With decreasing sample size, the shear deformation becomes more significant, thus stabilizing the shear band and improving the plastic strain at failure. The fragmentation fracture is attributed to the low Poisson's ratio v of the Fe-based BMG. The size effect on the competition between shear fracture and fragmentation can be well explained by the critical shear offset and the energy density dissipated on the shear fracture surface.

Experimental

Ingots with the composition of $Fe_{57.6}Co_{14.4}B_{19.2}Si_{4.8}Nb_4$ were prepared by arc melting a mixture of the pure elements in an argon atmosphere. The ingots were then re-melted for several times until a homogenous melt was formed. The final BMG rods with a diameter of 2.0 mm were produced by ejection copper mold casting. The microstructures and the phases of the prepared ingots were characterized with a Leo Supra 35 scanning electron microscope (SEM), as well as by X-ray diffraction using a Rigaku diffractometer with Cu Kα radiation. The final ingots exhibit only broad diffraction maxima without peaks of crystalline phases, revealing the amorphous structure of the samples. Compression test samples with two dimensions were prepared from the identical as-cast 2 mm diameter BMG rods. One group of samples had a diameter of 2.0 mm and a height of 4.0 mm (Sample S1), and the other group of samples was 1.0 mm in width and 2.0 mm in height (Sample S2). The lateral surfaces of each sample were polished by 1.5 µm diamond paste. Uniaxial compression tests were performed with an MTS810 testing machine at room temperature using a constant strain rate of about 1×10^{-4} s^{-1}. All tests were repeated for more than 3 times. Afterwards, the samples were observed by SEM to reveal the deformation features.

[1] W. L. Johnson, *MRS Bull.* **1999**, *24*, 42.

[2] A. Inoue, *Acta Mater.* **2000**, *48*, 279.

[3] W. H. Wang, C. Dong, C. H. Shek, *Mater. Sci. Eng. R* **2004**, *44*, 45.

[4] Z. F. Zhang, F. F. Wu, G. He, J. Eckert, *J. Mater. Sci. Technol.* **2007**, *23*, 747.

[5] Z. F. Zhang, G. He, J. Eckert, L. Schultz, *Phys. Rev. Lett.* **2003**, *91*, 045504.

[6] Z. F. Zhang, H. Zhang, B. L. Shen, A. Inoue, J. Eckert, *Philos. Mag. Lett.* **2006**, *86*, 643.

[7] Z. F. Zhang, J. Eckert, *Phys. Rev. Lett.* **2005**, *94*, 094301.

[8] W. J. Wright, R. Saha, W. D. Nix, *Mater. Trans.* **2001**, *42*, 642.

[9] Z. F. Zhang, J. Eckert, L. Schultz, *Acta Mater.* **2003**, *51*, 1167.

[10] X. K. Xi, D. Q. Zhao, M. X. Pan, W. H. Wang, Y. Wu, J. J. Lewandowski, *Phys. Rev. Lett.* **2005**, *94*, 125510.

[11] Q. J. Chen, J. Shen, D. L. Zhang, H. B. Fan, J. F. Sun, *J. Mater. Res.* **2007**, *22*, 358.

[12] G. Wang, D. Q. Zhao, H. Y. Bai, M. X. Pan, A. L. Xia, B. S. Han, X. K. Xi, Y. Wu, W. H. Wang, *Phys. Rev. Lett.* **2007**, *98*, 4.

[13] G. Chen, M. Ferry, *J. Mater. Sci.* **2006**, *41*, 4643.

[14] Z. F. Zhang, F. F. Wu, W. Gao, J. Tan, Z. G. Wang, M. Stoica, J. Das, J. Eckert, B. L. Shen, A. Inoue, *Appl. Phys. Lett.* **2006**, *89*, 251917.

[15] J. Shen, W. Z. Liang, J. F. Sun, *Appl. Phys. Lett.* **2006**, *89*, 3.

[16] X. K. Xi, D. Q. Zhao, M. X. Pan, W. H. Wang, Y. Wu, J. J. Lewandowski, *Appl. Phys. Lett.* **2006**, *89*, 181911.

[17] D. G. Pan, W. Y. Liu, H. F. Zhang, A. M. Wang, Z. Q. Hu, *J. Alloys Compds* **2007**, *438*, 142.

[18] D. G. Pan, H. F. Zhang, A. M. Wang, Z. G. Wang, Z. Q. Hu, *J. Alloys Compds* **2007**, *438*, 145.

[19] S. Puech, J. J. Blandin, J. L. Soubeyroux, *Adv. Eng. Mater.* **2007**, *9*, 764.

[20] X. K. Xi, D. Q. Zhao, M. X. Pan, W. H. Wang, Y. Wu, J. J. Lewandowski, *Phys. Rev. Lett.* **2005**, *94*, 125510.

[21] A. Inoue, B. L. Shen, C. T. Chang, *Acta Mater.* **2004**, *52*, 4093.

[22] B. L. Shen, A. Inoue, C. T. Chang, *Appl. Phys. Lett.* **2004**, *85*, 4911.

[23] G. Wang, Y. T. Wang, Y. H. Liu, M. X. Pan, D. Q. Zhao, W. H. Wang, *Appl. Phys. Lett.* **2006**, *89*, 121909.

[24] C. A. Pampillo, *J. Mater. Sci.* **1975**, *10*, 1194.

[25] Y. C. Kim, J. C. Lee, P. R. Cha, J. P. Ahn, E. Fleury, *Mater. Sci. Eng. A* **2006**, *437*, 248.

[26] Y. J. Huang, J. Shen, J. F. Sun, *Appl. Phys. Lett.* **2007**, *90*, 081919.

[27] T. Zhang, H. Men, S. J. Pang, J. Y. Fu, C. L. Ma, A. Inoue, *Mater. Sci. Eng. A* **2007**, *449–451*, 295.

[28] P. Yu, Y. H. Liu, G. Wang, H. Y. Bai, W. H. Wang, *J. Mater. Res.* **2007**, *22*, 2384.

[29] J. Lu, G. Ravichandran, *J. Mater. Res.* **2003**, *18*, 2039.

[30] F. F. Wu, B. L. Shen, Z. F. Zhang, S. X. Mao, **2008**, unpublished.

[31] J. J. Lewandowski, W. H. Wang, A. L. Greer, *Philos. Mag. Lett.* **2005**, *85*, 77.

[32] W. H. Wang, *J. Appl. Phys.* **2006**, *99*, 093506.

[33] H. Bei, S. Xie, E. P. George, *Phys. Rev. Lett.* **2006**, *96*, 105503.

[34] F. F. Wu, Z. F. Zhang, F. Jiang, J. Sun, J. Shen, S. X. Mao, *Appl. Phys. Lett.* **2007**, *90*, 191909.

[35] C. A. Pampillo, H. S. Chen, *Mater. Sci. Eng. A* **1974**, *13*, 181.

[36] L. A. Davis, S. Kavesh, *J. Mater. Sci.* **1975**, *10*, 453.

[37] J. J. Lewandowski, A. L. Greer, *Nat. Mater.* **2006**, *5*, 15.

[38] B. Yang, P. K. Liaw, G. Wang, M. Morrison, C. T. Liu, R. A. Buchanan, Y. Yokoyama, *Intermetallics* **2004**, *12*, 1265.